Onset and Saturation of a Non-Resonant Internal Mode in NSTX and Implications for AT Modes in ITER

J. Breslau, M.S. Chance, J. Chen, G. Fu, S. Gerhardt, N. Gorelenkov, S.C. Jardin, J. Manickam
Princeton Plasma Physics Laboratory, P.O. Box 451, Princeton, NJ 08543 USA

Abstract

Motivated by experimental observations of apparently triggerless tearing modes, we have performed linear and nonlinear MHD analysis showing that a non-resonant mode with toroidal mode number n=1 can develop in the National Spherical Torus eXperiment (NSTX) at moderate normalized β_N when the shear is low and the central safety factor q_0 is close to but greater than one. This mode, which is related to previously identified "infernal" modes, will saturate and persist, and can develop poloidal mode number m=2 magnetic islands in agreement with experiments. We have also extended this analysis by performing a free-boundary transport simulation of an entire discharge and showing that, with reasonable assumptions, we can predict the time of mode onset.

1. Introduction

One of the phenomena presenting an obstacle to successful plasma confinement in tokamaks is the seeding of neoclassical tearing modes (NTMs) [1], slow-growing resistive instabilities that create poloidal mode number m=2, toroidal mode number n=1 magnetic islands at the q=2 surface. In the National Spherical Torus eXperiment (NSTX), these have been observed to degrade energy confinement and to interact with resonant components of the intrinsic field coil error to exert a braking effect on plasma rotation, leading to mode locking. As the rotation slows, equilibria with normalized plasma pressure β above the no-wall limit become unstable to resistive wall modes (RWMs), causing disruption.

Often, the mechanism for the destabilization of the NTMs is apparent from the diagnostic data; they are observed to be triggered by sawteeth, energetic particle modes, edge-localized modes (ELMs), and by other locked modes. For a particular subset of NSTX discharges, however, the 2,1 mode amplitude begins to grow steadily from zero without any evident precursor in the soft X-ray, magnetic, or neutron diagnostic data [2]. A typical example of this class is shot #124379 (FIG. 1a). An important clue to the origin of the mode in this shot is that the multichord soft X-ray signal at time t=0.73 during the instability is best accounted for by the presence of a 1,1 kink-type perturbation in addition to the 2,1 perturbation (FIG. 1b). The equilibrium reconstruction for this snapshot exhibits a very flat central q profile with q_0 slightly above one. This suggests that the falling safety factor may be putting the plasma in a regime that is ideally unstable to a kink-like mode; the tight aspect ratio and high elongation of the spherical torus configuration could then couple the 1,1 mode to an m=2 component.

In this paper we perform numerical linear stability analysis of the equilibrium with a number of ideal and resistive MHD codes, verifying that this intuitive picture is correct: it is near marginal stability for an ideal n=1 mode with various poloidal components. We investigate the nonlinear behavior of the mode with a resistive MHD model, showing how it can saturate at finite amplitude for suitable choices of parameters. We also consider corrections to this analysis arising from the inclusion of kinetic effects of the hot ion population introduced by neutral beam injection (NBI), and discuss our attempts to simulate the time of onset of this mode using a discharge evolution transport code.

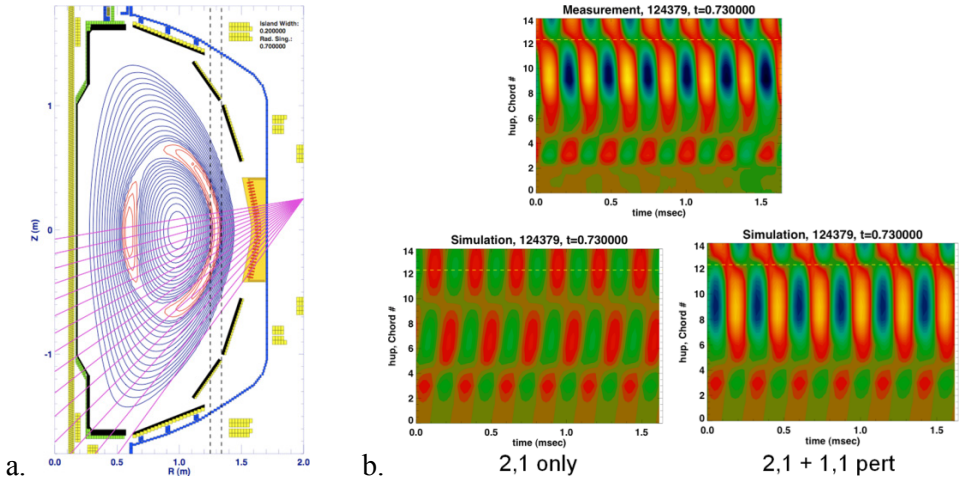

FIG 1: a. Diagram showing reconstructed island equilibrium and positions of USXR chords for NSTX shot 124379, t=*0.730. b. Comparison of simulated perturbed plasma state with and without (1, 1) component to measured multichord signal.*

2. MHD Stability

2.1 Equilibrium construction

We began our analysis with an LRDFIT equilibrium of NSTX discharge 124379 at time 640 ms, approximately the time of the mode onset. This had β_N=3.33 and I_P = 1 MA. In order to conduct more systematic scaling studies to clarify the physics of the mode, we also defined a parametrizable family of analytic equilibria to be computed by the JSOLVER code [3], an iterative fixed-boundary Grad-Shafranov solver that computes ideal axisymmetric MHD equilibria for specified analytic pressure and current profiles; it can be configured to target a particular central safety factor q_0, total plasma current I_p, or loop voltage V. Typical input parameters for the NSTX equilibria are given in Table I. The pressure profile was specified to be $p(\hat{\psi}) = p_0(1-\hat{\psi})$, where the radial coordinate $\hat{\psi}$ is the normalized poloidal flux. The current profile was given by

$$\frac{< \boldsymbol{J}.\boldsymbol{B} >}{< B.\nabla\varphi >} \propto \left(1-\hat{\psi}\right)^4 \tag{2.1}$$

which provides an extremely flat q profile in the center; additional off-axis current broadening terms taking the general form $J_{\|} \propto \left[\Delta^2\hat{\psi}(1-\hat{\psi})\right]/\left[(\hat{\psi}-a)^2+\Delta^2\right]$were added to provide the slightly reversed shear profile shown in FIG. 2.

TABLE I: INPUT PARAMETERS FOR THE JSOLVER EQUILIBRIUM CALCULATION

Major radius	0.8579 m
Minor radius	0.6022 m
Elongation	2.15
Triangularity	0.52
Toroidal field	0.4429 T
$\beta_0 \equiv 2\mu_0 p_0/B_0^2$	0.54
q_0	1.0 – 1.4

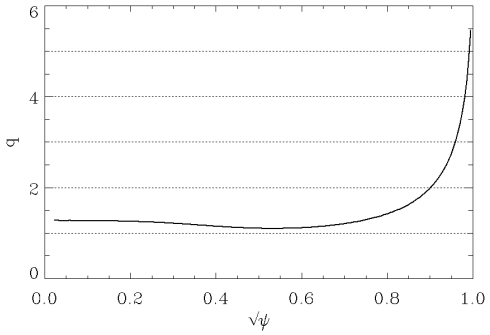

FIG. 2: q profile of the analytic NSTX equilibrium computed by JSOLVER after rescaling the field by a Bateman factor of 1.05.

2.2 Ideal stability

Ideal stability of the JSOLVER equilibria were evaluated using the PEST-1 code [4], which uses a variational method to minimize the Lagrangian for axisymmetric equilibria, yielding eigenvalues and displacement eigenvectors for all unstable modes. Only those equilibria found by PEST to be ideally unstable to n=1 modes but stable to n=2,3 were retained for further analysis. These proved to be modes with q_{min} slightly less than those in the experimental equilibrium reconstruction but still slightly above unity, in the range of 1.05–1.1. The most promising had q_0=1.25, q_{min}=1.074, and a PEST n=1 eigenvalue of $\lambda = \omega^2\tau_A^2 = -4.56 \times 10^{-3}$. As a benchmark exercise, this equilibrium was also evaluated with the nonvariational ideal stability code NOVA, and the results were in agreement.

2.3 Resistive stability

Linear numerical analysis was also performed with the M3D [5] and M3D-C^1 [6] codes. Both are initial-value finite element fluid codes capable of solving the complete set of resistive MHD equations using a stream-function/potential representation of the poloidal velocity field and a vector potential representation of the magnetic field. The relatively new M3D-C^1 code is fully implicit and uses a higher-order and more accurate set of basis functions, but to date lacks the ability to perform 3D nonlinear simulations. Both codes possess the ability to rescale their input equilibria taking advantage of the fact that in the Grad-Shafranov equation

$$\Delta^*\psi + \mu_0 R^2 \frac{dp}{d\psi} = -F\frac{dF}{d\psi} = -\frac{1}{2}\frac{d}{d\psi}(F^2), \tag{2.2}$$

the toroidal field F can be rescaled without changing the toroidal current density or pressure profiles simply by scaling its value at the boundary $\hat{\psi} = 1$ by Bateman factor B [7] and then integrating F^2 in to the axis using the existing profiles. This has the effect of rescaling the q profile in a way approximately proportional to B, and so is a convenient way to perform a parameter scan in q_0. When this is done with the M3D-C^1 code using the LRDFIT reconstruction of the NSTX equilibrium, the results indicate that the equilibrium is unstable to a very weakly growing resistive n=1 mode but is close to marginal stability to an ideal mode with both m=1 and m=2 components (FIG. 3). We find that the linear stability properties and the nonlinear development of this mode depend sensitively not only on the central value of the q-profile, but also on the central magnetic shear. If the shear is too low, higher-n modes become unstable before the n=1 as the central q value drops during the discharge evolution.

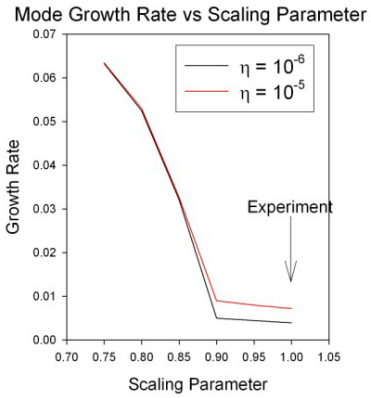

FIG. 3: Resistivity dependence of scaling of n=1 growth rate with q_0 for a family of TSC equilibria as computed by M3D-C^1.

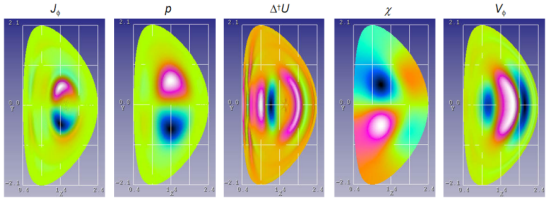

FIG. 4: Contours of the perturbed toroidal current density, velocity divergence, vorticity, toroidal velocity, and pressure in the n=1 eigenmode computed by M3D for the reconstructed JSOLVER equilibrium (B=1.05).

Growth rates and eigenmodes computed by M3D were consistent with those found by M3D-C^1 and, in the ideally unstable regime, with PEST and NOVA. The unscaled JSOLVER equilibrium described in section 2.2 above(q_{min}=1.074) was predicted to have an n=1 growth rate of $\gamma\tau_A = 4.1 \times 10^{-2}$, where τ_A is the poloidal Alfvén transit time. For B=0.9 (q_{min}=1.016), the growth rate increases to 5.6×10^{-2}; while for B=1.05 (q_{min}=1.101, FIG. 2), $\gamma\tau_A$ decreases to 1.9×10^{-2} and the eigenmode is as shown in FIG. 4, predominantly 1,1 but with a 2,1 component. Like PEST and NOVA, M3D predicted the n=2 and n=3 modes to be stable.

3. Nonlinear simulations with M3D

The linear n=1 eigenmodes computed by the M3D code for the respective Bateman-scaled JSOLVER equilibria were scaled up to a perturbed kinetic energy of 5×10^{-8} in code units and used as initial states for time-dependent nonlinear three-dimensional calculations with the same code. Resistivity profiles took the form $\eta(\boldsymbol{x}, t) = \eta_0(T/T_0)^{-3/2}$ for various choices of η_0; viscosity was uniform at 5×10^{-4}; thermal conductivities were $\chi_\perp = 5 \times 10^{-5}$ and $\chi_\parallel = 0.5$; and a parallel hyperviscosity of the form

$$\frac{\partial \mathbf{V}}{\partial t} = \cdots - \mathcal{H}_\mu \frac{\partial^4 \mathbf{V}}{\partial \varphi^4} \tag{3.1}$$

was imposed to prevent spurious nonlinear growth of the high n modes, with $\mathcal{H}_\mu = 10^{-3}$. A time-centered version of the implicit shear Alfvén operator [8] was employed to allow larger time steps. Mesh resolution was 101 radial by 500 poloidal by 24 toroidal zones. A dealiasing filter retained only toroidal modes $n \leq 7$.

Nonlinear behavior of a typical instability over the course of 500 τ_A (a few hundred μs) is shown in FIG. 5. The n=1 mode begins to grow at its linear rate, causing a 1,1 kink to develop in the field structure. The mode quickly couples to higher-n modes. At some finite helical displacement, the mode saturates – the magnetic energy stops growing and the kinetic energy begins to decay – leaving the plasma in a state with (2, 1) magnetic islands of some fixed size, in qualitative agreement with the experimental discharge.

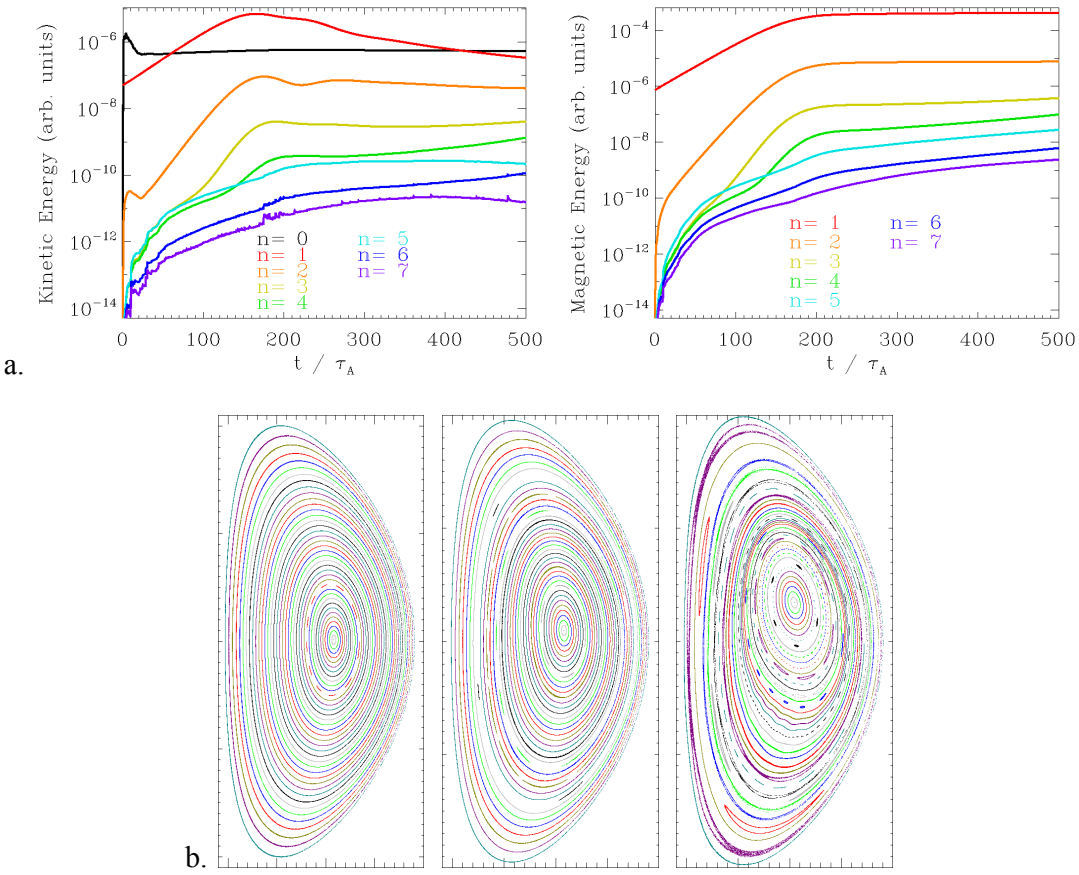

FIG. 5: Nonlinear saturation of the ideal n=1 mode in NSTX. a. Kinetic and magnetic energy time histories by toroidal mode number. b. Poincaré plots of magnetic surfaces at φ=0 in initial (t=0), linearly growing (t=100), and saturated (t=250) states.

The dependence of the saturated state on equilibrium properties and on resistivity was investigated in a set of parameter scans, summarized in Table II. Because the n=1 mode is ideal, the dependence of its growth rate on resistivity was found to be weak. Reducing the resistivity does, however, have a stabilizing effect on modes $n \geq 5$, suggesting that the dominant mode may be driving a resistive ballooning instability in this high-β case. The linear growth rate and final vertical displacement of the axis (which are strongly correlated with each other) show much higher sensitivity to $\delta q \equiv q_{min} - 1$. This implies that quantitative validation with the experiment will require a very precise measurement of the q profile at mode onset. Little variation in saturated 2,1 island width was detectable over the scanned parameter range.

TABLE II: SCALING OF NONLINEAR SATURATION AMPLITUDE WITH q_{min} AND η_0

q_{min}	η_0	$\gamma\tau_A$	Vertical axis displacement (minor radii)	Saturated 2,1 island width (normalized flux units)
1.016	5×10^{-5}	5.51×10^{-2}	+0.822	3.118×10^{-2}
1.074	5×10^{-5}	3.45×10^{-2}	+0.526	2.623×10^{-2}
1.074	1.25×10^{-5}	3.49×10^{-2}	+0.538	2.810×10^{-2}
1.101	5×10^{-5}	1.79×10^{-2}	+0.322	2.618×10^{-2}
1.101	6.25×10^{-6}	1.85×10^{-2}	+0.358	2.882×10^{-2}

4. Kinetic Effects

4.1 Perturbative computations

To study the stabilizing effects of NBI ions on the n=1 ideal mode in NSTX, we use the perturbative code NOVA-K, which computes quadratic form terms including beam ion particles

$$\delta K = \delta W \equiv \delta W_{MHD} + \delta W_{kbeam}, \qquad \delta K = \omega^2 \int \rho \xi^2 d^3 r \tag{4.1}$$

based on the n=1 mode structure computed by the NOVA code without fast particles. Unlike the ideal MHD case, where $\delta K \sim \omega^2$, the assumption that $\delta K \sim \omega$ can be substituted, which produces the following dispersion relation [9] to account for the fast particle kinetic potential energy:

$$-i\omega \left(1 + \frac{\omega_T^2}{\omega_s^2 - \omega^2}\right) = \gamma_{MHD} \left(1 + \frac{\gamma_{beam}}{\gamma_{MHD}}\right), \ \frac{\gamma_{beam}}{\gamma_{MHD}} = \frac{\mathcal{R}\delta W_{kbeam}}{\delta K}, \tag{4.2}$$

where $\omega_T^2 = 2\gamma_s P_c \kappa/\rho$, $\omega_s^2 = (1/2)\gamma_s \beta_c \omega_A$, κ is the curvature, $\gamma_s = 5/3$, and ρ is the plasma mass density. One can see that the real part of the fast particle contribution to the potential energy $\mathcal{R}\delta W_{kh}$ can give stabilization and is computed in NOVA-K according to the following formula [10], which includes particle finite orbit width (FOW) and finite Larmor radius (FLR) effects:

$$\delta W_{kbeam} = -(2\pi)^2 e_\alpha c \int dP_\varphi d\mu d\mathcal{E} \tau_b \sum_{m,m',l} \frac{X^*_{m,l}(\omega - \omega_*) X_{m',l}}{\omega - \overline{\omega_d}} \frac{\partial F_{beam}}{\partial \mathcal{E}}, \tag{4.3}$$

where the integration is performed over the particle phase space $P_\varphi, \mu, \mathcal{E}$ in general tokamak geometry, τ_b is the particle bounce time, $X_{m,l}$ gives the wave-particle interaction power exchange, F_{beam} is the fast particle equilibrium distribution function, $\omega_* = -i \frac{\partial F/\partial P_\varphi}{\partial F/\partial \mathcal{E}} \frac{\partial}{\partial \varphi}$, and ω_d is the particle toroidal drift frequency. Once can see from Eq. (4.3) that the condition $\omega < \omega_d$ is required for the mode stabilization to occur. In other words, since the n=1 mode frequency is associated with plasma diamagnetic frequency ω_* and $\omega_d \sim \mathcal{E}$, particles should be energetic enough for $\omega_* < \omega_d$ to provide the stabilization.

4.2 NSTX simulations with NOVA-K

In these simulations we use the Lorentz form of the scattering collision operator for the equilibrium distribution function model [11], which is characterized by two parameters: injection pitch angle $\chi_0 = 0.55$; and the width of the distribution in pitch angle at the injection $\Delta\chi = 0.3$. We also used the TRANSP-generated plasma profiles, which are close to those used in the M3D simulations but more unstable. In NOVA simulations with no-wall boundary conditions, only the n=1 mode was found to be unstable, which is consistent with the M3D results.

Results of the simulations for beam ion stabilization are summarized in FIG. 6. They are sensitive to the q_{min} of the safety factor profile. At the inferred values of q_{min} = 1.25 the ideal mode is strongly unstable and the fast ions do not contribute much to its stabilization. Only near the threshold of the instability is the stabilizing effect from beam ions strong, q_{min}=1.53. Nevertheless, it seems that beam ions can play in important role near the threshold of the

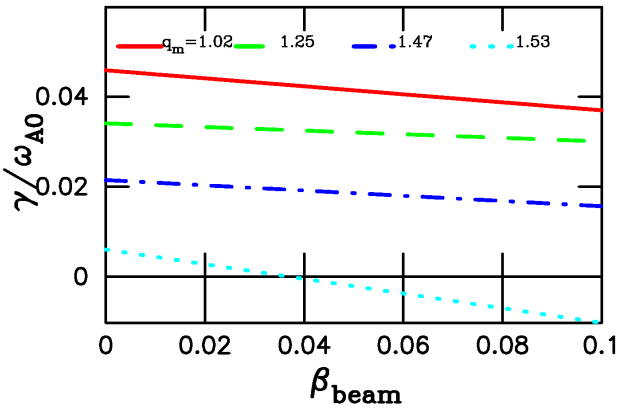

FIG 6: Growth rate of ideal mode stabilized by beam ions in NSTX. Experimental value of beam ion beta is $\beta_{beam} = 10\%$.

instability via the redistribution and affecting the beam contribution to the current drive and to the q profile.

5. Discharge evolution

In order to see if we could predict the onset time of the mode, we used the TSC free boundary transport code [12] together with the NUBEAM Monte-Carlo neutral beam code coupled through the CSWIM IPS framework [13]. A new option, using TRXPL, allows us to import the density and/or pressure profiles from a previous TRANSP run into the simulation and to use these instead of the predictive profiles computed by TSC. We find that if we import both the pressure and density profiles, but use NUBEAM to compute the neutral beam current drive, and TSC to compute the bootstrap current and current profile evolution as well as the evolving equilibrium, we can reproduce the onset time for the unstable mode to within a few milliseconds. This gives some confidence that we could predict the onset of a similar mode in ITER if a reliable model for density and temperature profile evolution existed.

6. Discussion

We have shown that the "triggerless" tearing mode observed in NSTX shot #124379 and others can be accounted for by an ideal n=1 MHD mode that is destabilized as $q_{min} \rightarrow 1$ during the current ramp-up. Linear calculations demonstrate that this mode has a 1,1+2,1 structure, in accord with the multichord SXR measurements. The low central magnetic shear of the equilibrium suggests that this is closely related to previously identified "infernal" modes [14,15], which have a similar character, and is likely the same as the "long-lived mode" recently identified in MAST [16]. In reference [2], it was reported that the onset threshold of the "triggerless" NTM, unlike those triggered by ELMs and energetic particle modes, was not sensitive to rotation shear at the q=2 surface. This is to be expected if the modes are caused by this non-resonant mechanism. While the time and space behavior of the electron and ion thermal conductivities remain a major source of uncertainty in this modeling, and the simulation thus far lacks two-fluid or neoclassical effects, we find that M3D can reproduce the experimentally observed onset and nonlinear saturation of this mode with reasonable assumptions. This predictive capability gives us some confidence that we can predict the onset of these modes in ITER.

In future work, we plan to delve further into the prediction of the saturated 2,1 island width, investigating the dependence of this quantity on the details of a wider range of

equilibrium profiles, including those in which the n=2 or 3 modes become unstable before the n=1, while incorporating more complete physical models including kinetic effects of energetic particles in the nonlinear simulations. Establishing the power-law-dependence of the island growth rate on η should also help to clarify the regime in which saturation occurs. It should also be instructive to follow up on the high-n resistive modes seen in the nonlinear results by checking for ballooning stability, and characterizing its dependence on heat conduction near the plasma edge.

Acknowledgments

The authors gratefully acknowledge Wonchull Park for helpful discussions . This work was supported by U.S. DOE Contract No. DE-AC02-09CH11466.

References

[1] LA HAYE, R.J., "Neoclassical tearing modes and their control", Phys. Plasmas **13** (2006) 055501.
[2] GERHARDT, S.P., et al., "Relationship between onset thresholds, trigger types and rotation shear for the m/n=2/1 neoclassical tearing mode in a high-β spherical torus", Nucl. Fusion **49** (2009) 032003.
[3] DELUCIA, J., et al., "An iterative metric method for solving the inverse tokamak equilibrium problem", J. Comput. Phys. **37** (1980) 183.
[4] GRIMM, R.C., et al., "Computation of the magnetohydrodynamic spectrum in axisymmetric toroidal confinement systems", in: Methods in Computational Physics, Vol. **16**, ed. J. Killeen (Academic Press, New York, 1976) 253.
[5] PARK, W., et al., "Plasma simulation studies using multilevel physics models", Phys. Plasmas **6** (1999) 1796.
[6] JARDIN, S.C., et al., "The M3D-C^1 approach to simulating 3D 2-fluid magnetohydrodynamics in magnetic fusion experiments", J. Phys.: Conf. Series **125** (2008) 012044.
[7] BATEMAN, G. and PENG Y.M., "Magnetohydrodynamic stability of flux conserving tokamak equilibria", Phys. Rev. Lett **38** (1977) 829.
[8] BRESLAU, J.A and FU, G.Y., "Implementation of an implicit shear Alfvén operator in the M3D code", Comp. Phys. Communications **181** (2010) 1661-1670.
[9] CHENG, C.Z., "Kinetic extensions of magnetohydrodynamics for axisymmetric toroidal plasmas", Phys. Rep. **211** (1992) 1-51.
[10] GORELENKOV, N.N., et al., "Fast particle finite orbit width and Larmor radius effects on low-n toroidicity induced Alfvén eigenmode excitation", Phys. Plasmas **6** (1999) 2802.
[11] GORELENKOV, N.N. et al., "Beam anisotropy effect on Alfvén eigenmode stability in ITER-like plasmas", Nucl. Fusion **45** (2005) 226-237.
[12] JARDIN, S.C., et al., "Dynamic modeling of transport and positional control of tokamaks", J. Comput. Phys. **66** (1986) 481-507.
[13] SCIDAC CENTER FOR SIMULATION OF WAVE INTERACTION WITH MHD, online at http://cswim.org.
[14] MANICKAM, J., et al., "Ideal MHD stability properties of pressure driven modes in low shear tokamaks", Nucl. Fusion **27** (1987) 1461.
[15] HASTIE, R.J., et al., "Stability of ideal and resistive internal kink modes in toroidal geometry", Phys. Fluids **30** (1987) 1756.
[16] CHAPMAN, I., et al., "Saturated ideal modes in advanced tokamak regimes in MAST", Nucl. Fusion **50** (2010) 045007.